Journal of Power Sources 493 (2021) 229690

Contents lists available at ScienceDirect

Journal of Power Sources

journal homepage: www.elsevier.com/locate/jpowsour

# Understanding the limitations of lithium ion batteries at high rates

Michael.J. Lain [a,*], Emma Kendrick [a,b]

[a] Warwick Manufacturing Group, University of Warwick, Coventry, CV4 7AL, UK
[b] School of Metallurgy and Materials, University of Birmingham, Birmingham, B15 2TT, UK

## HIGHLIGHTS

- Harvested electrodes are tested at high discharge and charge rates.
- Several limiting processes were observed within a single 10 s pulse.
- In 10s pulses, the cathodes could be charged at 10C and stay below the 4.2 V limit.
- The anodes voltages went negative at 5C, but the limiting process was diffusion.
- Repeated pulsing with 20C, 10s pulses lead to lithium plating on the anodes.

## ARTICLE INFO

*Keywords:*
Lithium ion
Power density
Rate limitation
Asymmetric diffusion
HEV

## ABSTRACT

Commercial lithium ion cells with different power: energy ratios were disassembled, to allow the electrochemical performance of their electrodes to be evaluated. Tests on coin cell half cells included rate tests (continuous and pulsed), resistance measurements, and extended pulse tests. Pulse power tests at high rates typically showed three limiting processes within a 10 s pulse; an instantaneous resistance increase, a solid state diffusion limited stage, and then electrolyte depletion/saturation. On anodes, the third process can also be lithium plating. Most of the cells were rated for a 10 C continuous discharge, and the cathode charging voltage at 10 C was around 4.2 V. For anodes, the maximum charge current to avoid a negative voltage was 3–5 C. Negative anode voltages do not necessarily mean that lithium plating has occurred. However, lithium deposits were observed on all the anodes after 5000 pulse sequences with 10 s pulses at ± 20 C.

## 1. Introduction

Lithium ion cells are being used in an increasingly wide range of applications. This has led to more specialisation in cell design, with some cells optimised for high energy density, and others for high power density. The latter are used in hybrid electric vehicles (HEV), power tools, and e-cigarettes. Previously [1], a group of commercial lithium ion cells were disassembled, to measure properties like the areal capacities, coating thicknesses, and electrode porosities. The electrodes recovered from these cells also present an opportunity to perform electrochemical tests. A key observation on the cell specifications was the high current ratings for discharge, but relatively low ratings for charge. This is not a particular concern for power tools, where one battery pack is charged while the spare is being used. Similarly, e-cigarette devices can be conveniently charged overnight, like mobile phones. However, it is an issue for HEV batteries, where a typical duty cycle involves high rate charge and discharge pulses [2]. In most HEV vehicles, some energy that could be used for regenerative charging is dissipated in the brakes, to protect the batteries from high rate charging [3]. Therefore, it is important to measure the performance of both electrodes at high rates of charge and discharge, to understand their fundamental limitations.

Charging lithium ion cells at high rates and/or low temperatures can be detrimental to both electrodes. At the graphite anode, there is a risk of lithium plating rather than intercalation, once the electrode voltage drops below 0 V vs. $Li/Li^+$. In some electrochemical systems, there is an over-potential required to nucleate metal deposits, which then grow more easily, at a lower over-potential [4]. Thus, a negative voltage does not necessarily mean that lithium will deposit. Lithium deposition and stripping has a lower coulombic efficiency than lithium intercalation and de-intercalation, once a stable solid electrolyte interphase (SEI) layer has formed. SEI material will form on each fresh lithium deposit. These processes will therefore consume active lithium and electrolyte. A

* Corresponding author.
*E-mail address:* m.j.lain@warwick.ac.uk (Michael.J. Lain).

https://doi.org/10.1016/j.jpowsour.2021.229690
Received 18 November 2020; Received in revised form 1 February 2021; Accepted 20 February 2021
Available online 11 March 2021

**Table 1**
Lithium ion cells included in this study.

| Manufacturer | Model | Size | Rated Capacity | Charge Current | Discharge Current/A | |
|---|---|---|---|---|---|---|
| | | | /A hr | /A | Continuous | Pulse |
| A123 | M1A | 18650 | 1.1 | 4.0 | 30 | N/A |
| LG | HB2 | 18650 | 1.5 | 4.0 | 30 | 45 |
| LG | HB4 | 18650 | 1.5 | 4.0 (6.0) | 30 | N/A |
| LG | HG2 | 18650 | 3.0 | 4.0 | 20 | 30 (95) |
| Samsung | 25R | 18650 | 2.5 | 4.0 | 20 | 100 |
| Samsung | 30Q | 18650 | 3.0 | 4.0 | 15 | 20 |
| Samsung | 48G | 21700 | 4.8 | 4.8 | 10 | 35 |
| Sony | VTC5A | 18650 | 2.5 | 2.5 | 30 | N/A |
| Sony | VTC6 | 18650 | 3.0 | 3.0 | 20 | N/A |

greater risk is the prospect of dendrites growing through the separator, creating an internal short circuit. Commercial 26650 cells with an LFP cathode were charged at low temperatures (– 26 °C to – 20 °C), to investigate lithium plating [5]. The differential plots dV/dQ and dQ/dV during discharge were analysed to differentiate between reversible and irreversible lithium plating. The highest reversibility measured was 93%, at – 20 °C and 60% state of charge.

For high rate charging at the cathode, there is a risk of forming a higher resistance phase around the predominantly hexagonal or rhombohedral phase particles [6]. A high rate charge pulse can lower the surface lithium concentration to the point at which irreversible phase change can occur. There are several examples of NMC materials, where rock-salt phases have been detected on the surface [7–10]. This can be associated with processes like transition metal dissolution and oxygen evolution. Continued high rate charging introduced cracks into NMC-622 particles [11].

"Harvested" electrodes have been used previously in cell development and characterisation studies [12–15]. The degradation mechanisms in 18650 cells were investigated after different cycling and storage tests [12]. The increase in cell resistance was mainly due to the NCA cathode ($LiNi_{0.8}Co_{0.15}Al_{0.05}O_2$ or $LiNi_{0.8}Co_{0.1}Al_{0.1}O_2$). Side reactions at the graphite anode consumed active lithium. Pouch cells containing LCO ($LiCoO_2$) cathodes and graphite anodes were stored under trickle charge at different temperatures [13]. The main capacity loss occurred at the anode, with lithium deposits detected after storage at higher temperatures. The performance of LCO and NCA cathodes was compared in 18650 cells, particularly during storage tests at 45 °C [14]. The LCO cathode lost much more capacity than the NCA cathode, or the graphite anode in either cell. The main difference was the thickness of the surface layer with a cubic/rock salt structure on the cathode particles. After two years of storage, the layer was 4 nm thick on NCA, but 9 nm on the LCO. There was also a 20 nm sub-surface layer on the LCO particles, with a mixed rock salt/α-$NaFeO_2$ structure. A variety of different disassembly and electrode processing approaches were investigated [15], to achieve consistent cycling performance in the coin cell tests.

In this work, we investigated the anodes and cathodes from nine commercial lithium ion cells, using a range of electrochemical techniques to determine the rate limiting processes. The cells were deliberately selected to give a range of different power: energy ratios, amongst cells from the same manufacturer. The cells included in this work are listed in Table 1, with various parameters taken from the manufacturers' data sheets [1]. All the anodes were based on graphite; the Sony, Samsung and LG HG2 anodes also contained some silicon particles. The A123 cathode used lithium iron phosphate (LFP) as the active material; all the other cathodes were layered metal oxides i.e. $LiNi_{0.8+\delta}Co_{0.15}Al_{0.05-\delta}O_2$ (NCA) and/or $LiNi_xMn_yCo_{1-x-y}O_2$ (NMC).

A variety of different electrochemical tests have been applied to the harvested electrodes, to measure their resistances and performance at high rates. Continuous discharge tests were performed at relatively low discharge rates. Measurements of area specific impedance (ASI) were made at different states of charge, and using different pulse durations [16]. The main technique used in this work was high rate current pulse tests, similar to the Galvanostatic Intermittent Titration Technique (GITT) [17–20]. The standard GITT involves a series of constant current pulses at different states of charge, hence the term titration. However, in most of the tests described here, the state of charge was fixed, and the current values were increased, to look for divergence from a solid state diffusion limited mechanism. The standard theory for GITT involves solving Fick's second law, using appropriate boundary conditions for the initial lithium concentration (uniform), and the flux at x = 0 (∝ current) and at x = L (zero). For a diffusion limited GITT transient, the voltage is proportional to $t^{0.5}$, and the effective diffusion coefficient can be calculated using:-

$$D^{0.5} = \frac{2IL}{\Pi^{0.5}} \cdot \left(\frac{dE}{dQ}\right) \cdot \left(\frac{dE}{dt^{0.5}}\right)^{-1} \quad t << L^2/D$$

In this equation, D is the diffusion coefficient, I is the current, L is the diffusion path length, E is the voltage and Q is the charge. If experiments are performed at a fixed state of charge, then the gradient ($dE/dt^{0.5}$) should be proportional to the current, since D, L and (dE/dQ) are

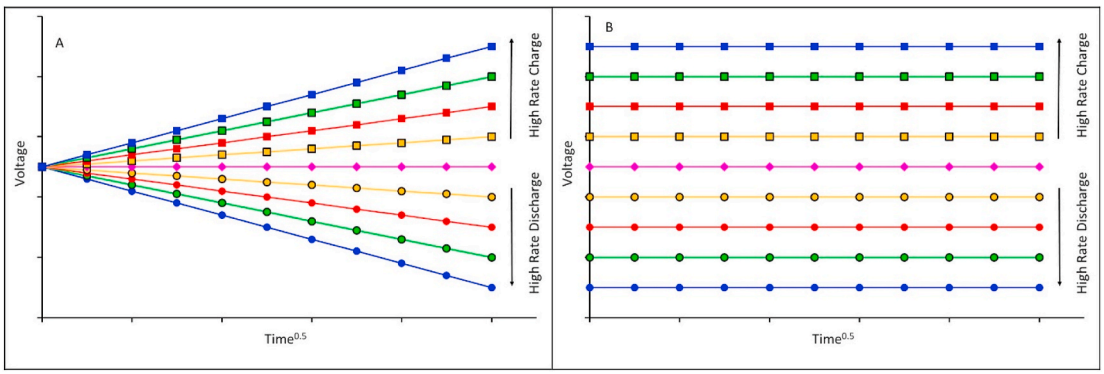


**Fig. 1.** Limiting responses to GITT tests at different rates A) diffusion limited. B) resistance limited.

invariant. The voltage transients can be used to distinguish between diffusion limited and resistance limited reaction mechanisms. The two limiting responses expected are plotted in Fig. 1. For diffusion limited processes, all the voltage transients start at the rest potential, with the gradient dependent on the current. For resistance limited processes, there is an immediate change in the voltage at the start of the pulse, given by Ohm's law, and then no further change. In practice, most of the results are a mixture of these two limiting cases, illustrating that electronic conductivity and ionic diffusivity both need to be maximised.

There are a number of experimental and modelling studies that investigate the various limiting processes within cells, generally with the aim of improving the performance at high rates. Almost invariably, these considered the total capacity during discharge at different rates. However, the limiting process during a short pulse may be different to a full discharge, and during charge different to discharge. Rate data from fifty published papers was extracted, and analysed using a consistent equation [21]. At high rates, the capacity was proportional to $(R\tau)^{-n}$, where R is the discharge rate, $\tau$ is the time constant of the rate limiting process, and n depends on the type of limiting process. In theory, $n = 0.5$ for a diffusion limited process, and $n = 1.0$ for a resistance limited process. In practice, values between $n = 0.5$ and 1.0 were common, and values $> 1.0$ were also obtained.

Time constants for different processes were an important part of the analysis of the rate performance of LTO anodes and NMC-111 cathodes [22]. The discharge capacities at higher rates decreased for thicker electrodes, implying that the limiting process was ionic diffusion in the electrode pores. When studying the effects of electrode thickness, it is important that the conductive carbon remains uniformly distributed, otherwise thicker electrodes will be compromised. For solid state diffusion in NMC, the diffusion path length was based on the size of the primary particles (0.8 μm), rather than the secondary particles (9 μm). Since $\tau = L^2/D$, this made two orders of magnitude difference to the calculated time constant. However, cross-sectional SEM images suggested there was minimal porosity in the secondary particles. This time constant approach was extended in further work, which developed the concept of a diffusion limited C rate or current [23,24].

Time constants also feature in a modelling investigation on the limiting processes in lithium ion cells [25], based on the pseudo two dimensional model (P2D) [26]. Three time constants were found to be important; for lithium transport in the electrolyte and the active materials, and for lithium ion depletion at the electrolyte/electrode interface, along with two resistance values in each electrode. If all three time constants were of similar magnitude, then the cell was not limited by the transport of any particular species. For thicker electrodes, the cell was limited by mass transport across the separator. At higher rates, the limitation was local depletion of the lithium ions around the active material particles. A similar modelling approach found a significant effect from electrode thickness at higher discharge rates [27]. Options to improve the rate performance included smaller particles of the active materials, and a higher lithium salt concentration in the electrolyte.

A comprehensive review of limiting processes in lithium ion cells focused on charge transfer reactions, rather than diffusion [28]. At each electrode, there is a series of process steps including desolvation of the lithium ion, transport though the SEI layer, and electron transfer. The paper states that electron transfer at the anode results in a lithium atom intercalated into the graphite. Spectroscopic data usually indicates that lithium in graphite is more ionic than atomic, so that the electron is transferred to and from the graphite, as with the transition metals in cathode materials. For example, EELS measurements on $LiC_6$ suggested that the lithium is closer to LiCl than to lithium metal, though LiCl is less fully ionised than LiF [29]. Similarly, modelling studies of silicon anode materials calculated that 70% of the electron charge sits on the silicon, with only 30% on the lithium [30]. Irrespective of the actual electron transfer mechanism, there are several possible limiting steps. Temperature can have a big influence on which one predominates, with the SEI resistance strongly temperature dependent.

A detailed investigation of the rate limitations of NMC, LFP and NMC + LFP cathodes used a combination of electrochemical and spectroscopic techniques [31]. Below a threshold rate, the capacity was limited by various contributions to the cell resistance. Above it, the limiting process was ionic diffusion into the electrode pore structure. There was a complicated interaction between the binder and carbon black contents and the tortuosity of the pore structure, as shown by x-ray tomography. Fast charging has been investigated in NCA/graphite cells, with impedance measurements of the individual electrodes facilitated by a lithium metal reference electrode [32]. Charge rates of up to 10 C could be used without lithium plating at the anode, because the cells had a high cathode to anode impedance ratio.

## 2. Experimental

The cylindrical lithium ion cells were discharged to their lower voltage limit, and then opened in an argon filled glove box. After unwinding the cell coil, the electrodes were immersed in anhydrous dimethyl carbonate (DMC) overnight, to remove any residual electrolyte, followed by drying at room temperature. Pieces of anode and cathode were transferred to the dry room (dew point < - 40 °C), inside a sealed container, as required. Most of the anodes showed some delamination during the initial unwinding, particularly on the inside winding close to the centre of the coil. Therefore, the pieces that were used to make coin cells were effectively single sided. There was much less delamination on the cathodes, so double sided pieces were used to make cells. This avoided any damage to the coating during the scraping of one surface. There is also relatively little current flow on the reverse side of the electrode, due to the relatively low conductivity of the electrolyte.

The electrodes were made into coin cell half cells, with a lithium metal counter electrode. The separator used was Celgard® H1609, and the electrolyte was 1 mol $dm^{-3}$ $LiPF_6$ in EC: EMC 3 : 7 wt%, with 2 wt% VC. For the extended pulse tests, a second separator layer of GF/A (glass fibre A) was used between the H1609 and the lithium metal. This minimised the risk of dendrite formation during the tests. The formation, rate tests, and ASI tests were performed on a BCS-805 unit, with channel limits of 0–5 V and ±150 mA. The high rate current pulse tests used a Maccor 4000 unit, with limits of - 2 V to +8 V, and ±5 A. For the graphite and graphite + silicon anodes, the voltage limits used were 0.005–1.5 V. The cathodes used 2.5–4.2 V, with a CC-CV charge protocol, apart from the A123 M1A cathode. This contains lithium iron phosphate (LFP) as the active material, so the limits were 2.5–3.95 V, with no constant voltage stage. All of the tests were performed at 25 °C, with the cells inside an environmental test chamber.

The test protocol used for area specific impedance (ASI) measurements was based on a paper [16] that under-pins the BatPac Model [33]. Following a full charge (lithiation), pulses were performed at every 10% state of charge (SoC). The pulses were a 10 s discharge at 1.8 C, followed by a 40 s rest, and then a 10 s charge at 1.2 C. The cells were allowed to rest for 1 h, after each change of state of charge. Further tests involved 2 s pulses at 50% SoC, and 30 s pulses at 20% SoC.

The high rate pulses were performed with the cells at a nominal 50% state of charge. The NMC and NCA cathodes were charged to 3.75 V, and anodes lithiated to 0.2 V, using CC-CV protocols. For the LFP cathode in the M1A cell, the cells were charged to 50% of the previously measured capacity. The test protocol used alternating discharge and charge pulses. A low rate charge or discharge pulse was used to return the SoC to the original value, before the next high rate pulse. The tests used a 30 min rest between each pulse, to ensure full relaxation before the next pulse, as 40 s rest was found to be insufficient. The twelve 2 s duration pulses were followed by twelve 10 s pulses.

Electrodes from the extended pulse tests were examined using a Hitachi TM3030 Tabletop scanning electron microscope (SEM), fitted with an Oxford Instruments Energy Dispersive Spectrometer (EDS) with a 30 $mm^2$ target area. After testing, the cells were disassembled in an argon filled glove box, and the electrodes were rinsed in anhydrous

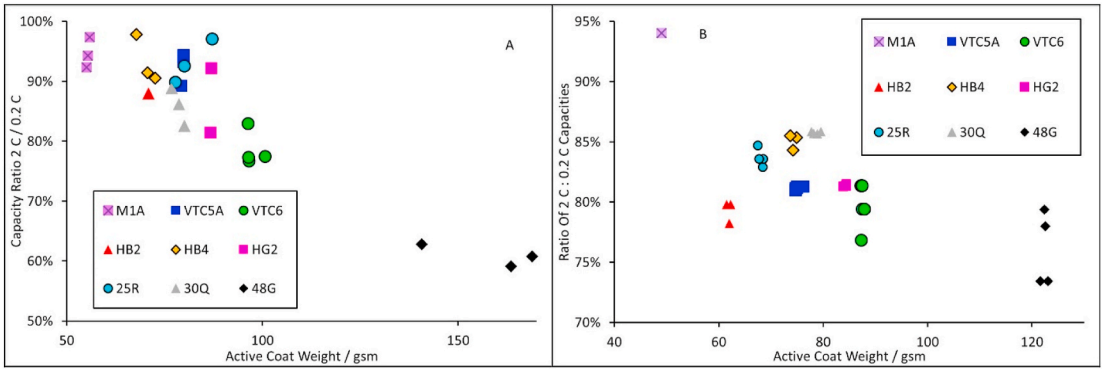


**Fig. 2.** Summary of rate tests using electrodes from different cells A) anodes and B) cathodes.

DMC. Segments of each electrode were sealed in bags for transfer to the analysis building. However, the electrodes were exposed to wet air for a few minutes during mounting on the SEM stubs, and placement in the SEM chamber.

## 3. Results and discussion

### 3.1. Rate tests (continuous)

All the original cells had been through the manufacturers' formation and ageing protocols, and at least one cycle. Some of the SEI components may have dissolved in DMC during the cell disassembly process, and others may have hydrolysed in the dry room. Therefore, the first test was a slow cycle at ± C/10, which was considered sufficient formation. This was followed by a series of rate tests, with a C/5 charge (lithiation) before each discharge (delithiation) at C/5, C/2, C or 2 C. Some typical results for each cell type are plotted in Figures S.1 and S.2, for anodes and cathodes respectively. There was a first cycle loss on the anodes, associated with the formation of a fresh SEI layer, in a generic rather than specific electrolyte.

A convenient method to analyse rate data is to plot the ratio of the discharge capacity at 2 C to the C/5 capacity, as shown in Fig. 2. At least three cells were made with each type of electrode. The spread in the points indicates variations in both coat weight and power capability, between nominally equivalent cells. For the anodes there was a clear, almost linear trend with coat weight. As already observed [1], cells with a high power: energy ratio have a lower areal capacity, which generally correlates with a lower coat weight. The Samsung 48G cell is optimised for maximum energy density, and therefore has the highest coat weight, and the poorest 2 C performance. The cathodes showed a similar relationship between 2 C: C/5 capacity ratio and the active coat weight. Again, the 48G cathodes had by far the highest coat weight. On average, the 2 C: C/5 ratios were lower for the cathodes than for the anodes. Only one M1A cathode cell is plotted, because the other three cells all had values > 100%. These cells needed more than one conditioning cycle to reach a stable capacity value, and were therefore excluded.

### 3.2. ASI measurements

After the rate tests had been completed, the cells were subjected to a series of pulses, to measure values for the area specific impedance (ASI). This is an important parameter when assessing the power of an electrode or cell, and is used in, for example, the BatPac model spreadsheet [33]. The individual cell results are plotted in Figures S.3 and S.4, for anodes and cathodes respectively. In these graphs, the blue points are the calculated ASI values for discharge (delithiation), and the red points were for charge (lithiation). The 2 s pulses at 50% gave slightly lower ASI values than the 10 s pulses, and the 30 s pulses at 20% SoC slightly higher.

To compare the results for the different cells, the ASI values for the 10 s pulses were averaged over a range of states of charge. These values are plotted in Fig. 3. With a fixed electrode formulation, the ASI is inversely proportional to the coating thickness, giving higher ASI values for thinner coatings and lower coat weights [16]. For these cells, the variations between different manufacturers, electrode formulations, and active materials were more important. To allow comparisons between the cells, the figures include lines differentiating between high, medium and low ASI values, calculated from the reciprocal of the coat weight. On this basis, the M1A cathode, VTC5A anode and HB4 anode had relatively low values, and the HB4 cathode, HG2 anode and 48G anode and cathode had relatively high values. As already observed, the 48G cell is optimised for energy density, and would therefore be expected to have higher resistance values. An interesting observation is that manufacturers do not always achieve low resistance at both electrodes; for example, the M1A cell (moderate anode, great cathode) and the HB4 cell (good anode, okay cathode).

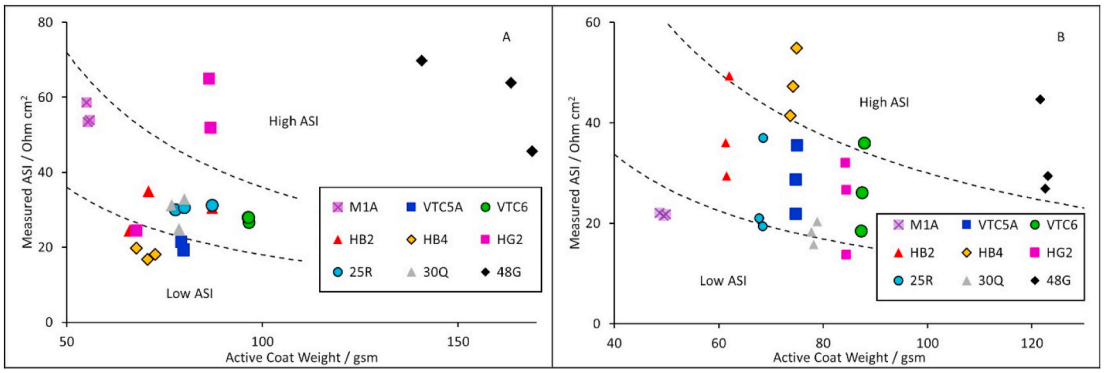


**Fig. 3.** Summary of ASI measurements in half cells using electrodes extracted from different cells for A) anodes and B) cathodes.

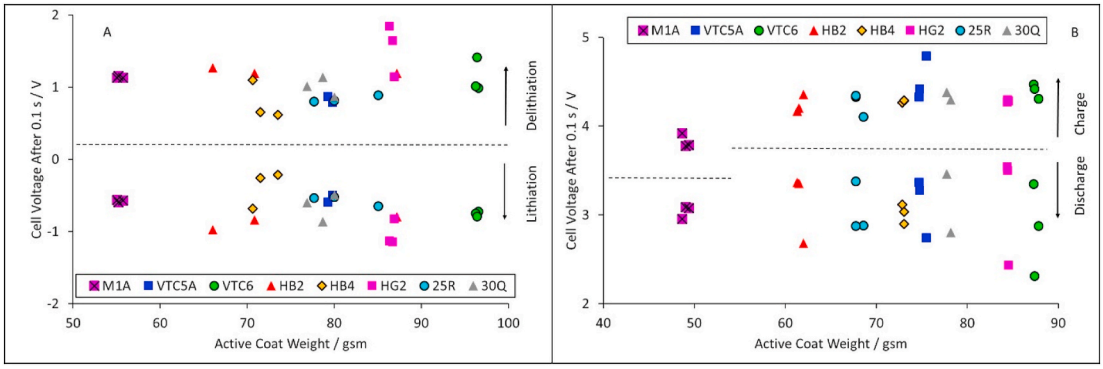


**Fig. 4.** Immediate voltage values for ±20 C pulse measurements A) anode and B) cathode.

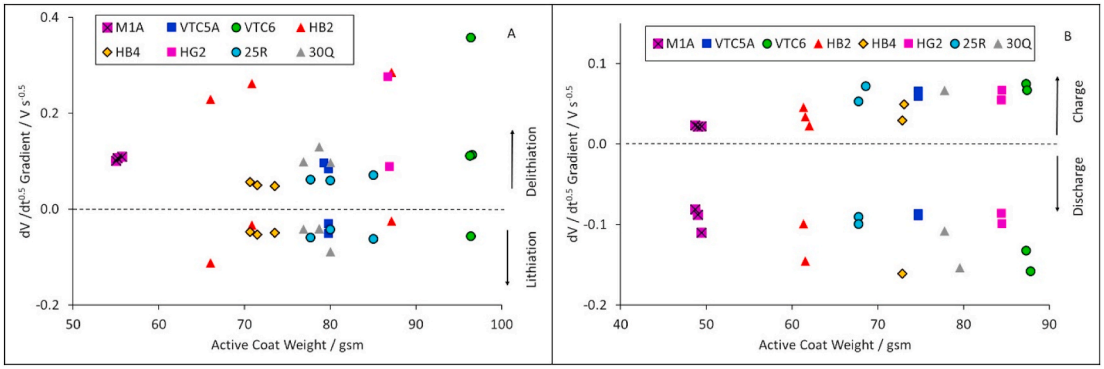


**Fig. 5.** Voltage gradients during ±20 C pulse measurements for A) anode and B) cathode.

### 3.3. Rate tests (pulse)

In HEV applications, the cells experience a series of high rate charge and discharge pulses, corresponding to periods of regenerative braking and acceleration. Therefore, it is more representative to test the electrodes under pulse conditions, rather than using a high rate continuous discharge. A series of 2 s pulses were performed, at increasing rates, followed by a matching series of 10 s pulses. The cells were nominally at 50% state of charge, and 25 °C. Using short pulses with an extended rest step between them avoids the issue of increasing cell temperature, which is often the limiting factor in high rate continuous discharges.

The experiments generated a large amount of data. Representative examples of voltage vs. $t^{0.5}$ plots for anodes and cathodes, during the 10 s pulses, are given in the supplementary information, Figures S.5 and S.6. At low rates of charge and discharge (lithiation and delithiation), there was good linearity in the plots. However, at higher rates, the voltages curved away from a straight line, suggesting that diffusion in the active materials was no longer the limiting process. Other limiting processes are discussed in greater detail later in this paper.

Another observation from the voltage transients is that the cells showed intermediate behaviour between the two limiting cases plotted in Fig. 1. There was an immediate voltage change at the start of the pulse (resistance), and then a continuing voltage change during the pulse (diffusion). Fig. 4 shows the voltages values after 0.1 s of the ±20 C pulses. The dotted lines show the voltage values at rest, before the start of the pulse. The results for the 48G cell were excluded from these graphs, because the voltage changes were significantly larger than the other eight cells. During lithiation, the initial anode voltages were below 0 V vs. $Li/Li^+$ at 20 C, and indeed even at 6.7 C. During delithiation, the voltages increased to around 1 V vs. $Li/Li^+$. The voltage changes seemed to be roughly symmetrical i.e. the charge and discharge resistances were equivalent. The voltage changes at the start of the charge and discharge pulses for the cathodes also seemed to be reasonably symmetrical.

**Table 2**
Maximum rates for harvested electrodes under diffusion control.

| Manufacturer | Cell | Anode | | Cathode | |
|---|---|---|---|---|---|
| | Type | Lithiation | Delithiation | Charge | Discharge |
| A123 | M1A | 20.0 | 10.0 | 20.0 | 30.0 |
| Sony | VTC5A | 20.0 | 20.0 | 13.7 | 10.0 |
| Sony | VTC6 | 13.7 | 10.0 | 13.7 | 10.0 |
| LG | HB2 | 13.7 | 10.0 | 20.0 | 20.0 |
| LG | HB4 | 6.7 | 10.0 | 6.7 | 20.0 |
| LG | HG2 | 13.7 | 20.0 | 13.7 | 10.0 |
| Samsung | 25R | 20.0 | 20.0 | 20.0 | 10.0 |
| Samsung | 30Q | 20.0 | 20.0 | 13.7 | 10.0 |
| Samsung | 48G | 1.2 | 1.8 | 6.7 | 5.0 |

During the charge pulses, the cell voltages jumped immediately to around 4.2 V.

Fig. 5 shows the gradients of voltage vs. $t^{0.5}$ during the linear region of the transient, again for ±20 C pulses. The results for the 48G cell were also excluded from these graphs, since the gradients were much higher than the other cells. The voltage gradients for the 48G cells during delithiation at 20 C were 2.0–3.6 V $s^{-0.5}$, compared to 0.1 V $s^{-0.5}$ for most of the other cells. Unlike the resistance measurements, the gradients of V vs. $t^{0.5}$ were not symmetrical, with smaller values during lithiation than delithiation for the anodes, and for charge than discharge, for the cathodes. The gradients of V vs. $t^{0.5}$ were calculated from the initial, linear section of the transient. In many of the measurements at higher rates, the voltages curved away from a straight line.

For some of the anode lithiation transients at 20 C, the gradient was positive, and these values are excluded from the Fig. 5. It seems unlikely that the positive gradients were caused by the onset of lithium plating, because the voltages eventually decreased. They could be caused by heating from the high localised current, which would reduce various

**Table 3**
Protocol designations for extended pulse tests.

| Protocol | Delithiation | | Lithiation | | Delithiation/s | | Lithiation/s | |
|---|---|---|---|---|---|---|---|---|
| | #1 | #2 | #3 | #4 | #1 | #2 | #3 | #4 |
| A1 | 20 C | 1.0 C | 20 C | 1.0 C | 10 | 35 | 10 | 35 |
| A2 | 20 C | 1.0 C | 20 C | 1.0 C | 2 | 43 | 2 | 43 |
| A3 | 2 C | 0.1 C | 2 C | 0.1 C | 10 | 35 | 10 | 35 |

resistances. They could also be due to the electrode relaxing after an initial shock at the start of the pulse. The maximum rates under diffusion control are collected in Table 2. For the M1A, VTC6, and HB2 anodes, the lithiation rate was higher than the delithiation rate. Similarly, for the VTC5A, VTC6, HG2, 30Q and 48G cathodes, the charge rate was higher than the discharge rate.

A number of observations and conclusions can be drawn from these experiments:-

- There was an immediate voltage change at the start of the pulse, due to the resistance contribution.
- For the anodes, the maximum lithiation rate that could be sustained above 0 V vs. Li/Li$^+$ was 3–5 C. However, higher rates could be sustained under diffusion control, which suggests that lithium plating might not actually be occurring. The cells were not dismantled to look for any evidence of lithium plating, because of the limited number and duration of the high rate pulses involved.
- For the cathodes, the maximum lithium rate that could be sustained below 4.2 V vs. Li/Li$^+$ was around 10 C. This is the maximum cell charging voltage, according to the data sheets. The LFP cathode in the M1A cell reached the 3.6 V cell charge limit at around 10 C.
- After the initial resistive increase, the electrodes then switched to a diffusion limited process, as indicated by the linearity of the voltage vs. $t^{0.5}$ plots.
- At higher rates of charge and discharge, a different limiting process took over part way through the 10 s pulses.
- There was asymmetry in the effective diffusion coefficients between charge and discharge, for both the anodes and cathodes, with faster diffusion during charge than discharge (at the cathodes) and for lithiation than delithiation (at the anodes).

### 3.4. Extended pulse tests

The previous section looked at single pulse tests at relatively high rates. However, in a real HEV application, the cells will experience thousands of charge and discharge pulses. Therefore, extended pulse test protocols were developed, to provide a more representative evaluation. Table 3 lists three anode half cell protocols, derived from the 90 s charge sustaining tests in a HEV test manual [2]. The pulse sequences were charge neutral, to maintain the initial state of charge. The delithiation voltage limit was reduced from +8 V to +3 V, to prevent copper dissolution. A complete set of 5000 pulse sequences lasted around five days, so overall this was a highly accelerated test.

In preliminary tests, protocol A3 caused minimal changes to the cell voltage and resistance, over the complete 5000 cycles. Protocol A2 caused some changes, with increased cell voltages during the 20 C delithiation step. However, protocol A1 was a much greater challenge. Therefore, it was decided to focus on this test, and look for differences across the range of available anodes. After a formation cycle, the anodes were lithiated to 0.15 V vs. Li/Li$^+$, before the start of the pulse sequences. A capacity check cycle was performed after the pulse tests. After the electrochemical testing, the cells were disassembled, and the

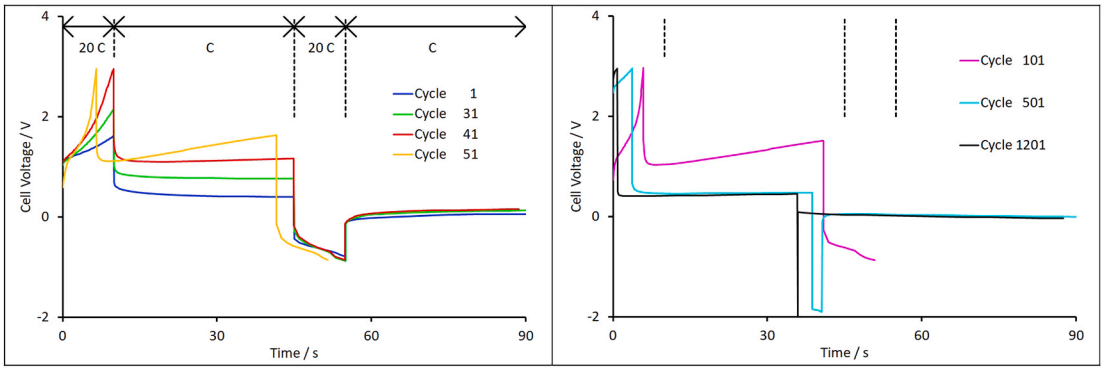


**Fig. 6.** Voltage transients for Samsung 30Q anode half cell.

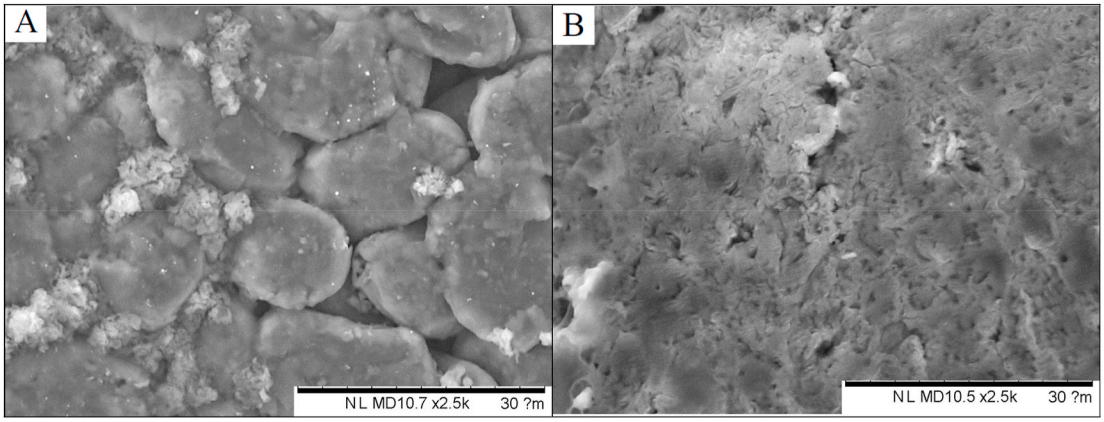


**Fig. 7.** SEM images of HB2 anodes after 5000 pulse sequences for A) graphite particles and B) "oxide" layer.

electrodes extracted for SEM/EDS analysis.

In most of the tests, there was a sequence of degradation steps. This is illustrated in Fig. 6, for a Samsung 30 Q anode. Equivalent graphs for all nine anodes are plotted in the Supplementary Information, Figure S.7. To keep the data files to manageable lengths, data was only recorded on every tenth pulse cycle. The stages were:-

- An increase in the cell voltage during the 20 C delithiation step (cycle 31).
- The cell voltage reached 3 V before 10 s, and the pulse was truncated (cycle 41).
- The C rate lithiation pulse was cut to maintain the state of charge (cycle 51).
- The 20 C lithiation pulse was shortened (cycle 501).
- Lithiation at 20 C was no longer possible (cycle 1201)

The point at which the anode could no longer be lithiated at 20 C was defined as the point of failure. The actual test times are collected in Table S.1. In every case, the pulse sequences were truncated by the voltage limits, and the average duration of the pulses sequences was much less than 90 s. The table also includes the delithiation capacities from the formation and post pulse capacity check cycles. Although the performance at high rates had been compromised, there was still some capacity for cycling at ± C/10.

When disassembled, all the cells showed silvery metallic deposits on top of the anode coating. Frequently, parts of this flaked off during handling, or transfer to the SEM. Where possible, SEM images and EDS maps were recorded in both the silvery and dark regions of the electrode. SEM images from both regions are shown in the Supplementary Information, Figures S.8 and S.9. Example SEM images for an HB2 anode are shown in Fig. 7. The dark regions were similar to the original coatings, as extracted. There were some lighter, wispy deposits in the pores of the electrode structures. These deposits could block ionic diffusion in the pores, and therefore reduce the rate capability of the electrode significantly.

The silvery SEM deposits were completely different. They formed a reasonably coherent layer on the original coating, though with some granular structure. They were classified as an “oxide” layer, because of the greatly increased oxygen content. Figure S.10 plots the carbon: oxygen ratios for three sample types; the original anode (~5 at% oxygen), the anode coating after the extended pulse tests (15–20 at% oxygen), and the oxide layer (>60 at% oxygen). The silvery deposit was almost certainly lithium metal. The extended pulse test protocol produced a relatively thick, dense deposit, rather than the dendritic lithium often observed. Unfortunately, lithium cannot be detected using standard EDS equipment. The sample transfer from the cell disassembly glove box to the SEM vacuum chamber minimised the exposure to air, but did not eliminate it. Therefore, any metallic lithium would have acquired an oxide coating.

### 3.5. Discussion

In almost every test at higher rates, the voltage vs. $t^{0.5}$ transients curved away from a straight line, during the 10 s pulses. For typical particle sizes and diffusion path lengths, it is very unlikely that the limit $t \ll L^2/D$ has been exceeded. Therefore, a different (tertiary) limiting process took over, during both charge and discharge, at each electrode. One candidate is voltage drop across the separator. However, the tertiary limiting process was observed at currents of only 50 mA $cm^{-2}$, and separate tests showed that the H1609 separator could operate up to at least 200 mA $cm^{-2}$.

One process that is known to cause sudden changes of voltage is salt depletion in the electrolyte. During high rate discharge, lithiation of the cathode can consume all the lithium ions in the electrolyte around the cathode particles. This causes a drop in ionic conductivity, and hence the electrode voltage. Similarly, during high rate charge, the same scenario

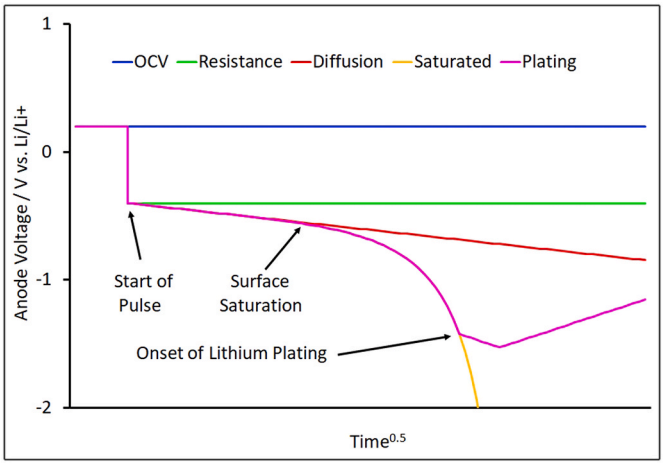


**Fig. 8.** Alternative limiting processes, with surface saturation and lithium plating.

can occur at the anode. However, this process only works in one direction at each electrode, and the limiting process was observed in both directions. Therefore, given that the limiting process occurs at both electrodes, in both current directions, the most likely explanation is that the surface concentration of lithium in the active material particles is either zero or 100%. If the delithiation current at a particle is faster than the diffusion flux can supply, then the surface concentration will eventually reach zero. The boundary condition used in the GITT model is that the current is proportional to the surface concentration gradient $I = nFAD.(\partial c/\partial x)_\sigma$ [17]. When the surface concentration reaches zero, the gradient will decrease, and the voltage will no longer follow the $t^{0.5}$ line. Similarly, during high rate lithiation, the surface concentration can rise to 100%, at which point the concentration gradient will again decrease. Illustrative concentration profiles are plotted in Figure S.11. This also has implications for lithium plating at the anode. Plating is usually considered to be a nucleation and growth process i.e. there is an energy barrier to create a nucleus of sufficient size to be stable, which can then grow much more easily. In these circumstances, anode voltages would be expected to decrease and then rise again. This is illustrated in Fig. 8. In practice, all the voltages went straight down to the machine limit of –2 V. Obviously, this does not prove that lithium plating did not occur during this particular pulse, but is does suggest that negative anode voltages do not automatically lead to lithium plating.

A similar interpretation was reached in pulse charging tests on graphite anode half cells [34]. The pulse durations were adjusted to keep the same change in state of charge for the different rates, from around 1 min at 10 C to 10 min at 1 C. The onset of plating was detected at around 15 s at 10 C, and 40 s at 5 C. Lithium plating produced a grey deposit, which revealed a “net like” structure covering the graphite particles under higher magnification. There was no indication of lithium plating during the 1 C pulse, even though the cell voltage was negative.

Overall, the proposed tertiary limiting mechanisms are:-

| | | |
|---|---|---|
| Anode | Lithiation | Saturation of lithium in surface layer of anode particles or Depletion of lithium salt in electrolyte next to particles |
| Anode | Delithiation | Depletion of lithium in surface layer of anode particles |
| Cathode | Charge | Depletion of lithium in surface layer of cathode particles |
| Cathode | Discharge | Saturation of lithium in surface layer of cathode particles or Depletion of lithium salt in electrolyte next to particles |

Another interesting observation was the asymmetry in the V vs. $t^{0.5}$ gradients between charge and discharge. To investigate this in greater detail, Table 4 collects values for charge and discharge gradients at ± 20 C, where these had the correct sign. It was possible to make a comparison of these gradients for fifteen electrodes. In thirteen of these tests, the gradient was noticeably higher during discharge than during charge

**Table 4**
Ratio of high rate pulse gradients at ± 20 C.

| Manuf. | Cell | Anode | | | Cathode | | |
|---|---|---|---|---|---|---|---|
| | | Lithiation | Delithiation | Ratio | Charge | Discharge | Ratio |
| | | /V $s^{-0.5}$ | /V $s^{-0.5}$ | /% | /V $s^{-0.5}$ | /V $s^{-0.5}$ | /% |
| A123 | M1A | N/A | 0.106 | N/A | 0.046 | −0.067 | 146 |
| Sony | VTC5A | −0.041 | 0.087 | 214 | 0.066 | −0.090 | 137 |
| Sony | VTC6 | −0.057 | 0.113 | 196 | 0.074 | −0.247 | 332 |
| LG | HB2 | −0.034 | 0.262 | 771 | 0.034 | −0.123 | 364 |
| LG | HB4 | −0.049 | 0.050 | 101 | 0.049 | −0.199 | 401 |
| LG | HG2 | N/A | 0.276 | N/A | 0.054 | −0.093 | 171 |
| Samsung | 25R | −0.060 | 0.061 | 103 | 0.053 | −0.095 | 180 |
| Samsung | 30Q | −0.042 | 0.099 | 237 | 0.038 | −0.154 | 399 |
| Samsung | 48G | −0.274 | 0.689 | 251 | N/A | −0.199 | N/A |

(for cathodes), and for delithiation compared to lithiation (for anodes). In the other two tests, the gradients were effectively the same. This is a clear example of asymmetric diffusion, which has two main causes; geometry and heterogeneous diffusion layers. In the former, the structure of the substrate makes diffusion easier in one direction than the other. For example, if the pores in an electrode are tapered, diffusion is faster from narrow to wide than vice versa [35]. More generally, it is easier to diffuse out from a lower porosity area to a higher porosity area [36]. Diffusion across two layers with different properties can also lead to asymmetric diffusion [37,38]. Frequently, there is a step change in concentration at the interface between the two layers.

Asymmetric diffusion has been observed here in anode and cathode half cells. At the cathodes, this could be due to geometric factors. During charge, lithium ions move out through the electrode pores, towards the separator. This should be easier than diffusion back into the electrodes, during discharge. However, the anodes have similar porous structures. Therefore, diffusion should be enhanced during delithiation over lithiation, which is the reverse of the experimental results. Thus, the diffusion process observed is more likely to be solid state diffusion in the active material particles, with asymmetric diffusion caused by heterogeneous layers. The anode SEI is known to form a coherent layer around the graphite particles. The lithium ion diffusion coefficient is likely to be different in the graphite and SEI, along with different layer thicknesses and concentrations of sites. The cathode interphase layer is much less well characterised, and is often considered patchy rather than coherent [39]. However, cathode particles often have surface layers with a different structure and/or composition from the bulk particles [6–10]. This can be caused by mild hydrolysis during cell manufacturing, or operation at high rates or to high voltages.

## 4. Conclusions

The aim of these experiments was to understand the limiting processes that occur in the electrodes from commercial lithium ion cells, especially during charging at high rates. This is a particular concern for HEV applications, where regenerative braking energy is wasted, to protect the batteries and extend their operating life. For this reason, short duration, high rate pulses were applied to the anodes and cathodes.

In half cell tests, the diffusion rates at both the anodes and cathodes were faster during charge than for discharge, which will help fast charging. This asymmetric diffusion is probably due to heterogeneous layers in the active materials i.e. the SEI layer on the anodes, and surface layers with a different structure on the cathode particles.

However, fast charging is likely to be restricted by the electrodes resistances. There was an immediate voltage change when the high rate pulses were applied. The maximum current that could be applied to the cathodes, at the rated charging voltage limit for the cells, was around 10 C. For the anodes, the limit was 3–5 C, before the voltage went negative of the lithium metal counter electrode. This introduces the possibility of lithium plating. Another issue is that the diffusion limited process could not be sustained through many of the high rate, 10 s pulses. This is most likely due to the lithium concentration at the surface of the particles reaching either 0% or 100%.

For all the anodes, lithiation at 6.7 C continued to be diffusion controlled, even though the electrode voltages were negative. There was no evidence of nucleation and growth of lithium particles in the voltage transients. However, it will be very difficult to reduce the resistance of the anode to the point at which the voltage does not go negative during high rate charging. Extended pulse tests did lead to lithium metal deposits, which tended to be coherent rather than dendritic. There was a surprising difference between the test protocols involving ±20 C/2 s and ±20 C/10 s pulses. The former caused steady increases in the electrode resistance, the latter damaged the electrodes very quickly.

## Funding statement

This work was undertaken as part of a contract with the Advanced Propulsion Centre (www.apcuk.co.uk). WMG gratefully acknowledge this funding from APC.

## CRediT authorship contribution statement

**Michael.J. Lain:** Conceptualization, Methodology, Investigation, Formal analysis, Data curation, Writing – original draft, Writing – review & editing. **Emma Kendrick:** Supervision, Writing – review & editing.

## Declaration of competing interest

The authors declare that they have no known competing financial interests or personal relationships that could have appeared to influence the work reported in this paper.

## Appendix A. Supplementary data

Supplementary data to this article can be found online at https://doi.org/10.1016/j.jpowsour.2021.229690.

## References

[1] M.J. Lain, J. Brandon, E. Kendrick, Design strategies for high power vs. high energy lithium ion cells, Batteries 5 (2019) 64, https://doi.org/10.3390/batteries5040064.
[2] INL/EXT-15-36567, USDoE Vehicle Technologies ProgramBattery test manual for 48V mild hybrid electric vehicles. https://dx.doi.org/10.2172/1389182.
[3] D. Peng, Y. Zhang, C.-L. Yin, J.-W. Zhang, Combined control of a regenerative braking and anti-lock braking system for HEVs, Int. J. Autom. Technol. 9 (2008) 749, https://doi.org/10.1007/s12239-008-0089-3.
[4] M. Matsui, Study on electrochemically deposited magnesium metal, J. Power Sources 196 (2011) 7048, https://doi.org/10.1016/j.jpowsour.2010.11.141.
[5] M. Petzl, M.A. Danzer, Non-destructive detection, characterisation and quantification of lithium plating in commercial lithium ion cells, J. Power Sources 254 (2014) 80, https://doi.org/10.1016/j.jpowsour.2013.12.060.

[6] D.P. Abraham, R.D. Twesten, M. Balasubramanian, I. Petrov, J. McBreen, K. Amine, Surface changes on LiNi0.8Co0.2O2 particles during testing of high power lithium ion cells, Electrochem. Commun. 4 (2002) 620, https://doi.org/10.1016/S1388-2481(02)00388-0.
[7] F. Lin, I.M. Markus, D. Nordlund, T.-C. Weng, M.D. Asta, H.L. Xin, M.M. Doeff, Surface reconstruction and chemical evolution of stoichiometric layered cathode materials for lithium ion batteries, Nat. Commun. 5 (2014) 3529, https://doi.org/10.1038/ncomms4529.
[8] H. Liu, M. Bugnet, M.Z. Tessaro, K.J. Harris, M.J.R. Dunham, M. Jiang, G. R. Goward, G.A. Botton, Spatially resolved surface valence gradient and structural transformation of lithium transition metal oxides in lithium ion batteries, Phys. Chem. Chem. Phys. 18 (2016) 29064, https://doi.org/10.1039/c6cp05262b.
[9] J. Li, H. Liu, J. Xia, A.R. Cameron, M. Nie, G.A. Botton, J.R. Dahn, The impact of electrolyte additives and upper cut-off voltage on the formation of rock-salt surface layer in NMC-811 electrodes, J. Electrochem. Soc. 164 (2017) A655, https://doi.org/10.1149/2.0651704jes.
[10] J.D. Steiner, L. Mu, J. Walsh, M.M. Rahman, B. Zydlewaki, F.M. Michel, H.L. Xin, D. Nordlund, F. Lin, Accelerated evolution of surface chemistry determined by temperature and cycling history of nickel rich layered cathode materials, Appl. Mater. Interfaces 10 (2018) 23842, https://doi.org/10.1021/acsami.8b06399.
[11] S. Xia, L. Mu, Z. Xu, J. Wang, C. Wei, L. Liu, P. Pianetta, K. Zhao, X. Yu, F. Lin, Y. Liu, Chemo-mechanical interplay of layered cathode materials undergoing fast charging in lithium batteries, Nano Energy 53 (2018) 753, https://doi.org/10.1016/j.nanoen.2018.09.051.
[12] D.P. Abraham, J.L. Knuth, D.W. Dees, I. Bloom, J.P. Christophersen, Performance degradation of high power lithium ion cells - electrochemistry of harvested electrodes, J. Power Sources 170 (2007) 465, https://doi.org/10.1016/j.jpowsour.2007.03.071.
[13] Q. Zhang, R.E. White, Calendar life study of lithium ion pouch cells, J. Power Sources 173 (2007) 990, https://doi.org/10.1016/j.jpowsour.2007.08.044.
[14] S. Watanabe, M. Kinoshita, K. Nakura, Capacity fade of NCA cathode for lithium ion batteries during accelerated calendar and cycle life tests. I. Comparison analysis between NCA and LCO cathodes in cylindrical lithium ion cells during long term storage test, J. Power Sources 247 (2014) 412, https://doi.org/10.1016/j.jpowsour.2013.08.079.
[15] A.U. Schmid, M. Kurka, K.P. Birke, Reproducibility of lithium ion cell reassembling processes and their influence on coin cell ageing, J. Energy Storage 24 (2019) 100732, https://doi.org/10.1016/j.est.2019.04.006.
[16] K.G. Gallagher, P.A. Nelson, D.W. Dees, Simplified calculation of the area specific impedance for battery design, J. Power Sources 196 (2011) 2289, https://doi.org/10.1016/j.jpowsour.2010.10.020.
[17] W. Weppner, R.A. Huggins, Determination of the kinetic parameter of mixed conducting electrodes and application to the system $Li_3Sb$, J. Electrochem. Soc. 124 (1977) 1569, https://doi.org/10.1149/1.2133112.
[18] W. Weppner, R.A. Huggins, Electrochemical methods for determining kinetic properties of solids, Annu. Rev. Mater. Sci. 8 (1978) 269, https://doi.org/10.1146/annurev.ms.08.080178.001413.
[19] C.J. Wen, B.A. Boukamp, R.A. Huggins, W. Weppner, Thermodynamic and mass transport properties of LiAl, J. Electrochem. Soc. 126 (1979) 2258, https://doi.org/10.1149/1.2128939.
[20] E. Markevich, M.D. Levi, D. Aurbach, Comparison between potentiostatic and galvanostatic intermittent titration techniques for determination of chemical diffusion coefficients in ion insertion electrodes, J. Electroanal. Chem. 580 (2005) 231, https://doi.org/10.1016/j.jelechem.2005.03.030.
[21] R. Tian, S.-H. Park, P.J. King, G. Cunningham, J. Coelho, V. Nicolosi, J.N. Coleman, Quantifying the factors limiting rate performance in battery electrodes, Nat. Commun. 10 (2019) 41467, https://doi.org/10.1038/s41467-019-09792-9.
[22] C. Heubner, J. Seeba, T. Liebmann, A. Nickol, S. Börner, M. Fritsch, K. Nikolwski, M. Wolter, M. Schneider, A. Michaelis, Semi-empirical master curve concept describing the rate capability of lithium insertion electrodes, J. Power Sources 380 (2018) 83, https://doi.org/10.1016/j.jpowsour.2018.01.077.
[23] C. Heubner, A. Nickol, J. Seeba, S. Reuber, N. Junker, M. Wolter, M. Schneider, A. Michaelis, Understanding thickness and porosity effects on the electrochemical performance of NMC-622 based cathodes for high energy lithium ion batteries, J. Power Sources 419 (2019) 1190, https://doi.org/10.1016/j.jpowsour.2019.02.060.
[24] C. Heubner, M. Schneider, A. Michaelis, Diffusion limited C rate: a fundamental principle quantifying the intrinsic limits of lithium ion batteries, Adv. Energy Mater. 9 (2019) 1902523, https://doi.org/10.1002/aenm.201902523.
[25] F. Jiang, P. Peng, Elucidating the performance limitations of lithium ion batteries due to species and charge transport through five characteristic parameters, Sci. Rep. 6 (2016) 32639, https://doi.org/10.1038/srep32639.
[26] J. Newman, K.E. Thomas-Alyea, Electrochemical Systems, third ed., Wiley, 2004.
[27] Z. Du, D.L. Wood III, C. Daniel, S. Kalnaus, J. Li, Understanding limiting factors in thick electrode performance as applied to high energy density lithium ion batteries, J. Appl. Electrochem. 47 (2017) 405, https://doi.org/10.1007/s10800-017-1047-4.
[28] T.R. Jow, S.A. Delp, J.L. Allen, J.-P. Jones, M.C. Smart, Factors limiting Li+ charge transfer kinetics in lithium ion batteries, J. Electrochem. Soc. 165 (2018) A361, https://doi.org/10.1149/2.1221802jes.
[29] F. Wang, J. Graetz, M.S. Moreno, C. Ma, L. Wu, V. Volkov, Y. Zhu, Chemical distribution and bonding of lithium intercalated graphite: identification with optimised EELS, ACS Nano 5 (2011) 1190, https://doi.org/10.1021/nn1028168.
[30] V.L. Chevrier, J.R. Dahn, First principles studies of disordered lithiated silicon, J. Electrochem. Soc. 157 (2010) A392, https://doi.org/10.1149/1.3294772.
[31] N. Besnard, A. Etiemble, T. Douillard, O. Dubrumfaut, P. Tran-Van, L. Gautier, S. Franger, J.-C. Badot, E. Maire, B. Lestriez, Multiscale morphological and electrical characterisation of charge transport limitations to the power performance of positive electrode blends for lithium ion batteries, Adv. Energy Mater. 7 (2017) 1602239, https://doi.org/10.1002/aenm.201602239.
[32] S.S. Zhang, Identifying rate limitation and a guide to design of fast charging lithium ion battery, InfoMat 2 (2020) 942, https://doi.org/10.1002/inf2.12058.
[33] P.A. Nelson, K.G. Gallagher, I. Bloom, D.W. Dees, Modelling the Performance and Cost of Lithium Ion Batteries for Electric Drive Vehicles. ANL-12/55, second ed., 2012, https://doi.org/10.2172/1209682.
[34] C. Uhlmann, J. Illig, M. Ender, R. Schuster, E. Ivers-Tiffée, In situ detection of lithium metal plating on graphite in experimental cells, J. Power Sources 279 (2015) 428, https://doi.org/10.1016/j.jpowsour.2015.01.046.
[35] R.S. Shaw, N. Packard, M. Schröter, H.L. Swinney, Geometry induced asymmetric diffusion, Proc. Natl. Acad. Sci. Unit. States Am. 104 (2007) 9580, https://doi.org/10.1073/pnas.0703280104.
[36] F.J. Valdés-Parada, J. Alvarez-Ramirez, A volume averaging approach for asymmetric diffusion in porous media, J. Chem. Phys. 134 (2011) 204709, https://doi.org/10.1063/1.3594549.
[37] B.I. Yakobsen, Asymmetric diffusion of a non-linear spatially inhomogeneous medium, Sov. Phys. JETP 62 (1985) 1055.
[38] J. Alvarez-Ramirez, L. Dagdug, M. Meraz, Asymmetric diffusion in heterogeneous media, Physica A 395 (2014) 193, https://doi.org/10.1016/j.physa.2013.10.027.
[39] K. Edström, T. Gustafsson, J.O. Thomas, The cathode electrolyte interface in the lithium ion battery, Electrochim. Acta 50 (2004) 397, https://doi.org/10.1016/j.electacta.2004.03.049.